Tellus (2000), 52A, 181–189
Printed in UK. All rights reserved

TELLUS
ISSN 0280–6495

Numerical simulations of Rossby–Haurwitz waves

By JOHN THUBURN[1]* and YONG LI[2], [1]*Department of Meteorology, University of Reading, PO Box 243, Earley Gate, Reading, RG6 6BB, UK;* [2]*Data Assimilation Office and Joint Center for Earth System Technology, NASA/Goddard Space Flight Center, Greenbelt, Maryland, USA*

(Manuscript received 21 June 1999; in final form 7 October 1999)

ABSTRACT

Simulations of Rossby–Haurwitz waves have been carried out using four different high-resolution numerical shallow water models: a spectral model, two semi-Langrangian models predicting wind components and potential vorticity respectively, and a finite-volume model on a hexagonal–icosahedral grid. The simulations show that (i) unlike the nondivergent case, the shallow water Rossby–Haurwitz wave locally generates small-scale features and so has a potential enstrophy cascade, and (ii) contrary to common belief, the zonal wavenumber 4 Rossby–Haurwitz wave is dynamically unstable and will eventually break down if initially perturbed. Implications of these results for the use of the Rossby–Haurwitz wave as a numerical model test case are discussed. The four models tested give very similar results, giving confidence in the accuracy and robustness of the results. The most noticeable difference between the models is that truncation errors in the hexagonal–icosahedral grid model excite the Rossby–Haurwitz wave instability, causing the wave to break down quickly, whereas for the other models in the configurations tested the instability is excited only by roundoff error at worst, and the Rossby–Haurwitz wave breaks down much more slowly or not at all.

1. Introduction

Rossby–Haurwitz waves are steadily propagating solutions of the fully nonlinear nondivergent barotropic vorticity equation on a sphere (Haurwitz 1940). They are described exactly by analytic formulas and so they are useful test cases for numerical models of the nondivergent barotropic vorticity equation. Although the shallow water equations do not have analogous analytic solutions, a Rossby–Haurwitz wave initial condition is expected to evolve in a very similar way to that in the nondivergent barotropic vorticity equation case. For this reason Rossby–Haurwitz waves have also been used to test shallow water numerical models (Phillips, 1959) and are among the seven standard shallow water model test cases proposed by Williamson et al. (1992).

Because there is no analytic Rossby–Haurwitz wave solution to the shallow water equations, the most obvious way to assess the accuracy of any numerical solution is by comparison with a reference solution computed using a higher resolution model, for example the spectral model reference solution provided by Jakob et al. (1993). The numerical solution should also have the correct stability properties; since the work of Hoskins (1973), Rossby–Haurwitz waves with zonal wavenumbers less than or equal to 5 are commonly believed to be stable, while those with zonal wavenumbers greater than 5 are believed to be unstable. The accuracy of a numerical solution is much more straightforward to assess for a stable flow than for an unstable flow, and for this reason Williamson et al. (1992) proposed using the zonal wavenumber 4 Rossby–Haurwitz wave.

* Corresponding author.
e-mail: swsthubn@met.rdg.ac.uk

Recent published model results show that the details of the true shallow water Rossby–Haurwitz wave evolution are still uncertain, and emphasize the need for a definitive solution to this test case. For example Bates et al. (1995) show significant differences among 5-day simulations using three different numerical models. Moreover, based on the results of Semazzi and Dekker (1994), they question the validity of using convergence with resolution of a single numerical model to estimate truncation errors. Also, Thuburn (1997) found that in extended integrations using a hexagonal–icosahedral grid shallow water model the Rossby–Haurwitz wave pattern broke down after about 15 to 20 days; it was not clear whether this was caused by numerical problems with the model or a dynamical instability of the true solution. There is some uncertainty over the ability of the high-resolution spectral reference solution to resolve these difficulties, since the spectral model requires the inclusion of a scale-selective dissipation term, typically a $\kappa\nabla^4$ acting on the prognostic variables, to avoid the build-up of grid-scale noise, and the numerical solution is sensitive, to some degree, to the strength of the tunable parameter κ and the scale-selectivity of the dissipation (Bates et al., 1995; Bates and Li, 1997). In particular, the optimal value of κ depends on the details of the flow, and generally a larger value of κ is needed when there is generation of small-scale features and a "cascade" of potential enstrophy towards unresolved scales. The Rossby–Haurwitz wave is generally assumed to maintain its wavelike structure and therefore not to involve a significant cascade to small scales.

In order to seek a definitive solution for the shallow water Rossby–Haurwitz wave test case we have carried out high-resolution simulations using four different numerical models. The consensus among the different models gives increased confidence in the accuracy and robustness of the results. At the same time, differences between results from the different models allow some comparison of their relative strengths and weaknesses. Our results show that (i) unlike the nondivergent case, and contrary to the usual assumption, the shallow water Rossby–Haurwitz wave does locally generate small-scale features, and consequently the scale-selective dissipation used for the Williamson et al. (1992) reference solution is weaker than optimal for the simulation of fields like potential vorticity, and (ii) the wavenumber 4 Rossby–Haurwitz wave is, in fact, unstable to a triad interaction that was not included in Hoskins's (1973) analysis, though it was discussed by Baines (1976) for the nondivergent barotropic vorticity equation. Some implications of these results for the use of the Rossby–Haurwitz wave test case will be discussed.

2. The Rossby–Haurwitz wave test case

The wavenumber 4 Rossby–Haurwitz wave test case is described in detail by Williamson et al. (1992); only a brief description is given here. The initial velocity field is nondivergent, with streamfunction

$$\psi = -a^2\omega \sin\phi + a^2K(\cos\phi)^4 \sin\phi \sin 4\lambda, \qquad (1)$$

where λ is longitude, ϕ is latitude, $a = 6.37122 \times 10^6$ m is the planetary radius, and $\omega = K = 7.848 \times 10^{-6}\,\mathrm{s}^{-1}$. In the nondivergent case, this flow pattern would propagate towards the east without change in form at an angular velocity close to $12^\circ\,\mathrm{day}^{-1}$. The initial height field is chosen to be in balance with the velocity field so that the initial divergence tendency is zero, with the minimum depth of 8×10^3 m occurring at the poles (Fig. 1).

The test case was run for at least 35 days for each model, and in some cases up to 100 days. Model fields were written out every day for the first 15 days and every 5 days thereafter in order to give a detailed view of the early stages of the evolution where Bates et al. (1995) found inter-model differences, and of the flow leading to the breakdown of the wave structure seen by Thuburn (1997).

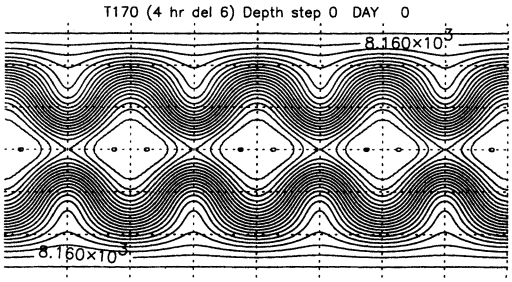

Fig. 1. Initial depth. Contour interval 120 m.

3. Numerical models

Four numerical models were used in this study: a spectral model, two grid-based models using semi-Lagrangian advection of wind components (UV semi-Lagrangian) and using semi-Lagrangian advection of potential vorticity (PV-D semi-Lagrangian), and a model based on finite volume (FV) methods using a hexagonal–icosahedral grid. The resolutions of the four models were chosen to be as similar to each other as possible. The models are described in detail in the references cited below. Only their most important characteristics are noted here.

The spectral model is a development of the model described by Hoskins (1973). The prognostic fields vorticity, geopotential height, and divergence are represented as series of spherical harmonics truncated at some maximum total wavenumber n, which defines the model resolution Tn. Nonlinear terms in the shallow water equations are evaluated efficiently by transforming fields to a grid representation. For the nondivergent barotropic vorticity equation the spectral model gives a very accurate simulation of the Rossby–Haurwitz wave because the solution is composed of only two, well-resolved, non-zero spherical harmonics. It is expected also to give a very accurate simulation in the shallow water case, even though the solution then contains other spherical harmonic components. Here a resolution T170 is used, with a corresponding grid of 512×256 points, and a time step of 300 s.

The UV semi-Lagrangian model is a shallow water version of the model described by Bates et al. (1993); see also Bates et al. (1995), and Li and Bates (1996). The two components of the wind vector and the geopotential height are represented on a regular longitude–latitude grid and are stepped forward in time using a semi-Lagrangian advection scheme. Here a resolution of 512×257 grid points is used with a time step of 3600 s.

The PV-D semi-Lagrangian model is described by Bates et al. (1995). Again, a regular longitude–latitude grid is used, and the predicted fields are stepped forward using semi-Lagrangian advection, though in this case those fields are potential vorticity, geopotential height, and divergence. Again a resolution of 512×257 grid points is used with a time step of 3600 s.

The FV model is described by Thuburn (1997). The model fields are represented on a grid of hexagonal and pentagonal grid cells that give uniform coverage of the sphere. A conservative, shape-preserving scheme is used to advect potential vorticity and depth. The third prognostic variable is divergence. Here a grid of 163842 cells is used, giving an average distance between cell centres of 60 km, and a time step of 225 s.

All four models use a semi-implicit treatment of the gravity wave terms, allowing stable integrations with longer time steps than would be possible with explicit time stepping. In addition, the two semi-Lagrangian models do not require advection-term Courant numbers less than 1 for numerical stability, and so can take time steps an order of magnitude longer than the spectral and FV models. Therefore, with the timesteps used, the two semi-Lagrangian models are roughly an order of magnitude cheaper computationally than the spectral and FV models.

As already noted above, the spectral model requires the inclusion of explicit scale-selective dissipation terms to avoid the build-up of grid-scale noise. All the integrations described here used a ∇^6 dissipation on all prognostic variables with a damping timescale of 4 h for the shortest retained scales. The other three models, however, use schemes that are inherently dissipative on small scales (McCalpin, 1988; Thuburn, 1995). They are able to soak up any cascade of potential enstrophy towards unresolved scales, preventing the build-up of grid-scale noise and giving stable integrations without the need for any explicit, tunable, scale-selective dissipation terms.

4. Results

4.1. *Evolution of depth field*

Fig. 2 shows the fluid depth from the spectral model simulation on days 3, 6, 9, and 12. The wave maintains its basic structure and propagates steadily eastward with a phase speed close to the analytic value for the nondivergent barotropic vorticity equation case. Superposed on this steady propagation are small vacillations in the wave structure. By day 3, the midlatitude troughs have become elongated and have acquired a poleward-westward tilt, implying an equatorward eddy momentum flux. By days 5 and 6, a closed 8520 m contour has appeared in each trough. By day 9,

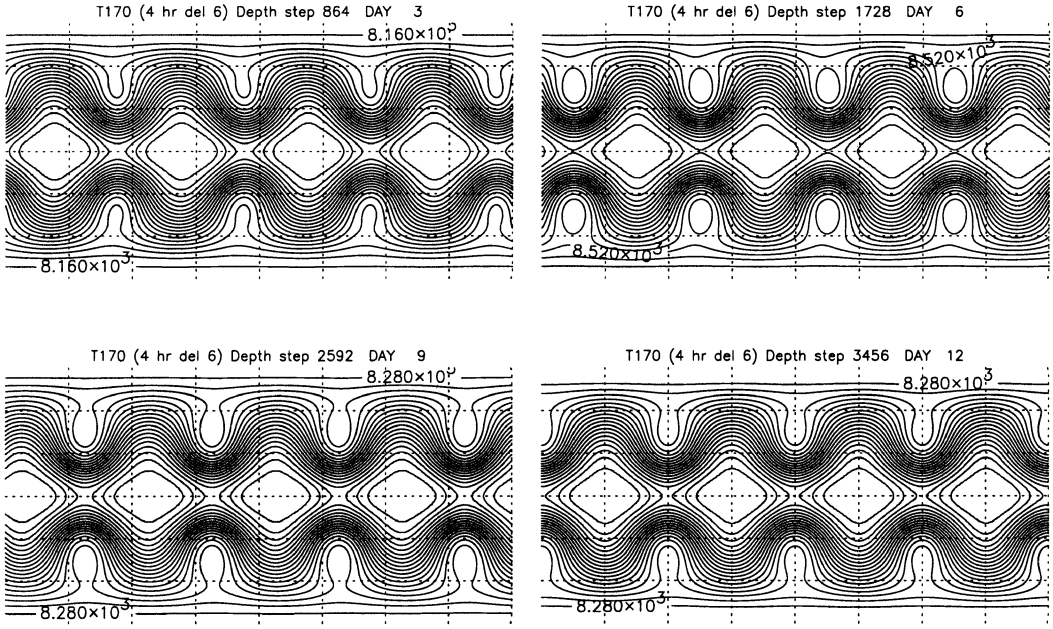

Fig. 2. Depth at days 3, 6, 9, and 12 from the spectral model simulation. Contour interval 120 m.

the 8520 m contour is no longer closed in each trough, and the troughs now have a slight poleward-eastward tilt implying a poleward eddy momentum flux. These details agree very well with the T213 spectral model solution of Jakob et al. (1993). These kinds of vacillation continue for the duration of the integration as long as the wave retains its basic structure, in this case out to day 50.

Results from the other three models agree remarkably well with those from the spectral model over the first 15 days. In all cases the wave maintains its basic structure and propagates steadily eastward, and even the details of the wave structure vacillations are very well reproduced. In particular, we could not reproduce the PV-D semi-Lagrangian model result of Bates et al. (1995), which was significantly different from their spectral and UV semi-Lagrangian model results by day 5. There are small differences in the simulated phase speeds, with that in the UV semi-Lagrangian model being about 0.3° day^{-1} slower than in the other models leading to a phase lag of about 4° by day 15. This phase lag is reduced when smaller time steps are used. It is related to the use of uncentering in the semi-Lagrangian time stepping (Li and Bates, 1996). In the PV-D model only the height and divergence equations use uncentering, not the PV equation, so that large-scale balanced flows are not significantly affected by the resulting phase lag.

Other differences between models include slight changes in timing of the wave structure vacillations; for example in the FV model the 8520 m contour remains closed on day 9 but opens by day 10. Also, small departures from the perfect zonal wavenumber 4 structure are visible in the FV model results, increasing as the integration proceeds. These are triggered initially by the distribution of truncation errors associated with the structure of the FV model grid, but, once triggered, they grow through a dynamical instability — see Subsection 4.3. Fig. 3 shows the geopotential height at day 15 from the four models. Even at day 15 the wave structure is very similar in all four models, and all are at the same stage of the wave structure vacillation. However, the departures from wavenumber 4 are clearly visible in the FV model results.

4.2. *Evolution of potential vorticity*

Fig. 4 shows potential vorticity (defined here as ζ/Φ, where ζ is the absolute vorticity and Φ is the

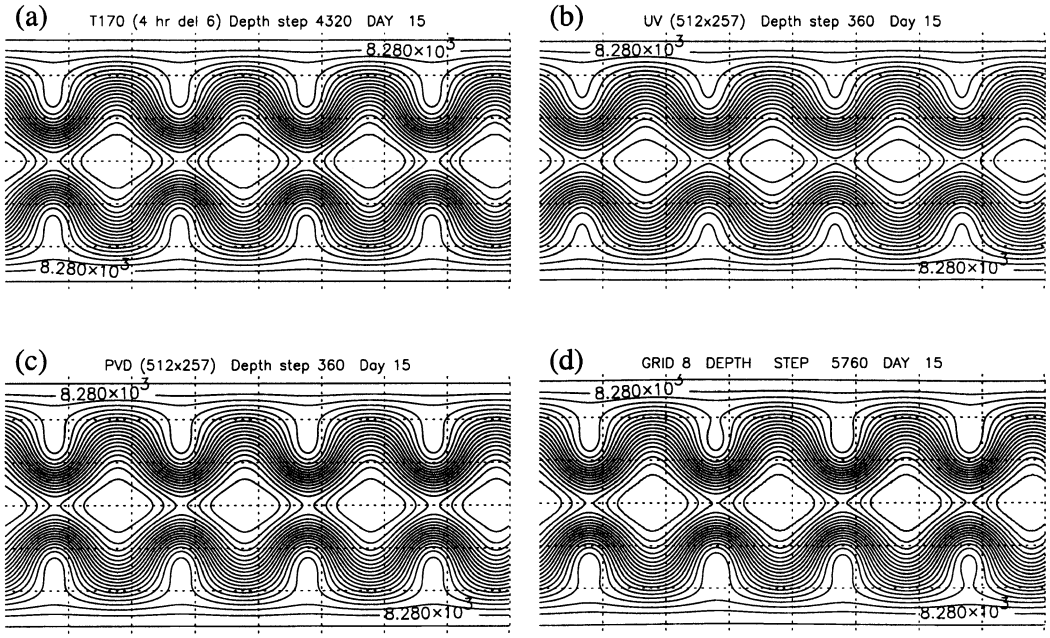

Fig. 3. Depth at day 15 from all four models. Contour interval 120 m. (a) Spectral model, (b) UV semi-Lagrangian model, (c) PV-D semi-Lagrangian model, (d) FV model.

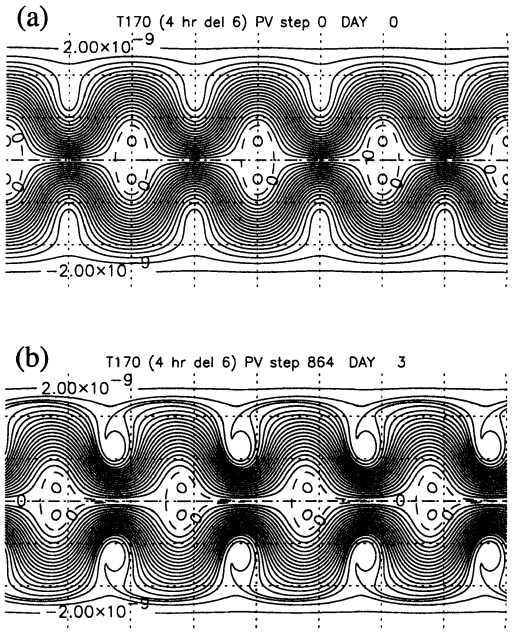

Fig. 4. (a) Initial potential vorticity and (b) spectral model potential vorticity at day 3. Contour interval $10^{-10}\,\mathrm{m}^{-2}\,\mathrm{s}$.

geopotential) at day 0 and day 3 from the spectral model integration and Fig. 5 shows potential vorticity from all four models at day 8. Although the initial potential vorticity field has an east–west symmetry about any of the troughs, over the first 3 days the troughs develop a poleward-westward tilt, consistent with the geopotential height structure, and tongues of potential vorticity values less than $1.8 \times 10^{-9}\,\mathrm{m}^{-2}\,\mathrm{s}$ are beginning to wrap cyclonically around the troughs. The wrapping up continues as long as the tongues can be resolved by the models, so that, for example, by day 8 the tips of the $1.8 \times 10^{-9}\,\mathrm{m}^{-2}\,\mathrm{s}$ contour tongues have made 2 complete revolutions about the trough centres.

This formation and wrapping up of potential vorticity tongues around the trough centres is qualitatively different from the behaviour in either analytic or numerical Rossby–Haurwitz wave solutions of the nondivergent barotropic vorticity equation. (Some tendency to wrap up can be induced in the nondivergent case by adding small perturbations to the initial conditions, but this tendency is far weaker and less robust than it is in the full shallow water case even without initial

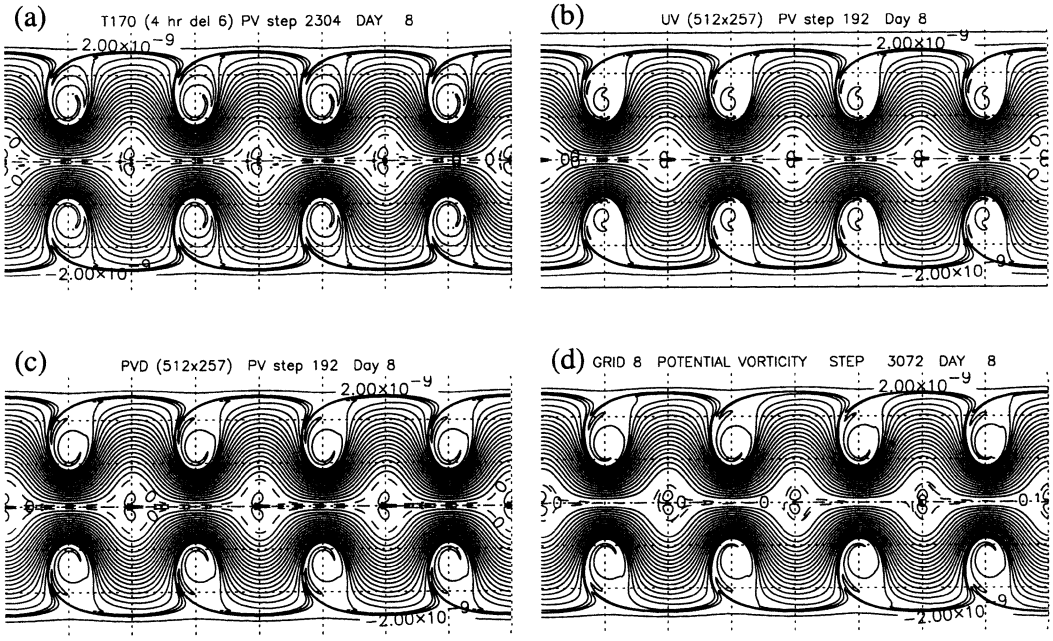

Fig. 5. Potential vorticity at day 8 from all four models. Contour interval $10^{-10}\,\mathrm{m}^{-2}\,\mathrm{s}$. (a) Spectral model, (b) UV semi-Lagrangian model, (c) PV-D semi-Lagrangian model, (d) FV model.

perturbations.) The agreement among the four models here gives confidence that the wrapping up is part of the true solution for the shallow water case. The initial velocity field is nondivergent and is defined such that the Jacobian $J(\psi, \zeta)$ vanishes, where ζ is the absolute vorticity and ψ is a stream function for the velocity in a frame of reference moving with the wave. The vanishing of this Jacobian is the condition that ensures that the flow pattern propagates without change of shape for the nondivergent barotropic vorticity equation. However, for the shallow water equations the corresponding condition is that $J(\psi, Q)$ should vanish, where Q is the potential vorticity, and this is not satisfied by the initial conditions. Inspection of contours of the initial ψ and Q shows that the initial tendency is to increase Q on the poleward-westward quadrant of the troughs and decrease it on the poleward-eastward quadrant, thereby establishing the tilt of the troughs and initiating the wrap up.

The formation and wrapping up of the potential vorticity tongues implies a generation of small scales and a cascade towards unresolved scales, albeit rather weak and localized. When this occurs numerical models require a mechanism to dissipate potential enstrophy near the grid scale as a proxy for allowing it to cascade to unresolved scales. Without such a dissipation mechanism potential enstrophy would build up near the grid scale leading to noisy structures in the solution, particularly in the potential vorticity field. For the spectral model we found that using dissipation with timescales longer than 4 h on the shortest retained scales led to noisy potential vorticity structures. In particular, the dissipation recommended by Jakob et al. (1993) (∇^4 with a timescale of about 10^5 s on shortest retained scales) is an order of magnitude too weak to maintain a noise-free potential vorticity field in this problem. The dissipation strength we used here is more typical of that used operationally in climate models.

The three other models have sufficient inherent dissipation to maintain noise-free potential vorticity fields. Arguably, it would be optimal for a model to have the minimum dissipation possible consistent with a noise-free solution. A crude measure of the relative dissipation strengths of the four models is given by the rate at which the tip of the $1.8 \times 10^{-9}\,\mathrm{m}^{-2}\,\mathrm{s}$ potential vorticity contour

tongues are eroded as they wrap up. This measure suggests that the dissipation strengths are very similar in the spectral, FV, and PV-D semi-Lagrangian models, being very slightly weaker in the spectral model with the particular value of dissipation coefficient used. The UV semi-Lagrangian model is a little more dissipative than the others. As with the phase errors discussed above, some of the dissipation in the UV semi-Lagrangian model is associated with the use of uncentering in the time stepping, and is reduced when shorter time steps are used (Li and Bates, 1996).

4.3. *Instability*

For the FV model, the departures from a perfect zonal wavenumber 4 pattern noted in Subsection 4.1 continue to grow until, between days 25 and 30, the wavenumber 4 pattern breaks down completely and the flow becomes turbulent (Fig. 6). Further experiments showed that this breakdown is accelerated at lower resolutions or when longer time steps are used. The spectral and PV-D semi-Lagrangian model solutions break down in a similar way, but at a much later time, between days 50 and 55 and between days 70 and 80, respectively. The UV semi-Lagrangian model solution, on the other hand, did not break down before day 100. A plausible explanation for this behaviour is that the Rossby–Haurwitz wave structure might in fact be susceptible to a dynamical instability: truncation errors associated with the grid structure of the FV model project onto the unstable mode so that it quickly grows to a significant amplitude; in the spectral and PV-D semi-Lagrangian models only roundoff errors project onto the unstable mode so that it takes longer to reach significant amplitude; in the UV semi-Lagrangian model neither truncation errors nor roundoff errors project onto the unstable mode so that it is never excited.

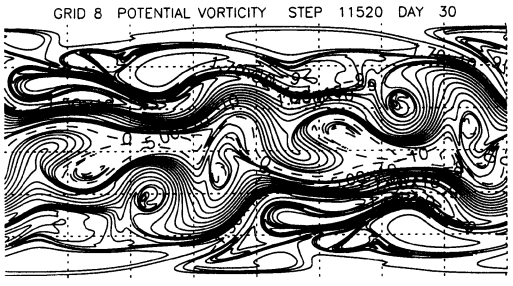

Fig. 6. Potential vorticity at day 30 from the FV model. Contour interval $10^{-10}\,m^{-2}\,s$.

To examine the stability of the Rossby–Haurwitz wave we carried out further experiments with the spectral model at T42 resolution in which small amplitude random perturbations were added to all spectral coefficients in the initial conditions. If the Rossby–Haurwitz wave is unstable then the initial perturbations should excite the instability and cause the wavenumber 4 structure to break down, and the time taken to break down will decrease as the amplitude of the initial perturbations is increased. This, indeed, is what happens; the wavenumber 4 Rossby–Haurwitz wave is unstable.

A likely mechanism for the instability is the triad interaction analysed by Baines (1976) for the nondivergent barotropic vorticity equation. Such triad interactions are well known in many kinds of fluid flows (Drazin and Reid, 1981). To examine this mechanism, Fig. 7 shows the contributions to the enstrophy (nondimensionalized using earth's rotation rate and radius) from different zonal wavenumber spectral components for one T42 spectral model solution. Between about day 10 and day 35 the contributions from wavenumbers

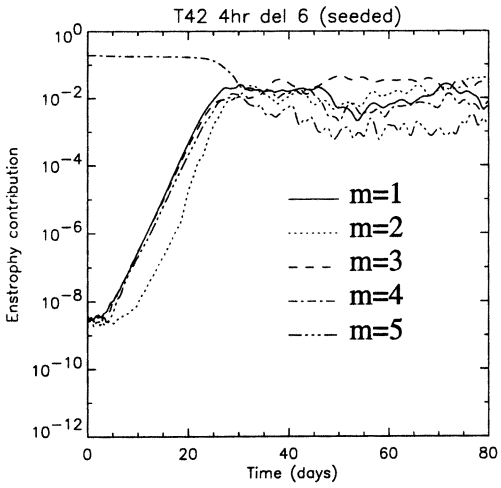

Fig. 7. Contributions to total enstrophy from zonal wavenumbers $m = 1$ to 5 from a spectral model simulation at T42 resolution with random perturbations added to the initial state.

1, 3, and 5 grow exponentially with an *e*-folding time of 1.3 days, indicative of normal mode growth in which the vorticity perturbations themselves have an *e*-folding time of 2.6 days. Similar growth curves are seen in both T42 and T170 integrations without the random initial perturbations, except that the growth of the $m = 1$, 2, 3, and 5 contributions begins around 10^{-15}, consistent with round-off errors, and takes much longer to reach a significant amplitude. These results are consistent with the mechanism of the instability being a triad interaction involving wavenumbers 1, 3, and 4 or wavenumbers 1, 4, and 5 (or possibly both sets). The weaker and less regular growth of wavenumber 2 could result from a combination of several possible wave–wave interactions, including wavenumbers 3 and 5, wavenumbers 2 and 4, and wavenumber 1 self interaction.

The involvement of wavenumbers 1, 3, and 5 in the instability explains why it was not captured in the analysis or numerical experiments of Hoskins (1973). Hoskins's analysis and experiments retained only zonal wavenumbers that were integer multiples of 4 and therefore excluded wavenumbers 1, 3, and 5. Hoskins himself noted that his analysis was valid only if his severe truncation was valid.

The instability of the Rossby–Haurwitz wave has implications for its use as a test case for numerical models. It implies that, for long enough integration times, solutions are strongly sensitive to small perturbations in initial conditions or to small numerical errors, and therefore we cannot expect agreement among different models and we cannot expect any single reference solution to be definitive. The breakdown of the wavenumber 4 flow pattern must be interpreted as a real dynamical instability triggered by small truncation or roundoff errors, not as a catastrophic failure of the numerical methods. Conversely, the fact that any particular model retains the wavenumber 4 structure without breakdown need not be interpreted as a special virtue, or shortcoming, of that model. It is simply a special case in which neither truncation nor roundoff errors project onto the instability, because the numerical model happens to possess the same symmetries as the initial Rossby–Haurwitz wave. In those cases it is almost certain that rotating the pole of the model grid to another latitude, or even using a number of longitudinal grid points that is not a multiple of 4, would be enough to excite the instability.

5. Summary

Numerical simulations of the zonal wavenumber 4 shallow water Rossby–Haurwitz wave have shown up two properties that have not been emphasized, and apparently not widely known, previously. (i) Unlike the nondivergent case, the shallow water Rossby–Haurwitz wave involves the generation of small-scale features in the potential vorticity field and therefore a potential enstrophy cascade. This has implications for the strength of scale-selective dissipation that must be used in numerical models, like spectral models, that need such dissipation in order to avoid noisy solutions. (ii) The zonal wavenumber 4 Rossby–Haurwitz wave is susceptible to a dynamical instability in which zonal wavenumbers 1, 3 and 5 grow. This has implications for the interpretation of results when the Rossby–Haurwitz wave is used as a numerical model test case.

During the first 15 days of the flow evolution, the four high-resolution numerical shallow water models tested gave very similar results. Small differences in detail in the potential vorticity field suggest that the UV semi-Lagrangian model is slightly more dissipative than the other models, while the spectral model, with the particular value of dissipation coefficient chosen, is very slightly less dissipative than the others. Also, the wave phase speed in the UV semi-Lagrangian model is slightly slower, by about $0.3^\circ\,\mathrm{day}^{-1}$, than in the other models.

In the FV model, small departures from the wavenumber 4 pattern, triggered initially by grid-related truncation errors but subsequently growing through the dynamical instability, begin to become visible in plotted fields by day 10. The wavenumber 4 pattern breaks down completely between days 25 and 30. We believe the same instability is triggered only by roundoff errors in the spectral and PV-D semi-Lagrangian models, and the wavenumber 4 pattern breaks down much later, between dayś 50 and 55 and between days 70 and 80, respectively. The instability is not excited in the UV semi-Lagrangian model. This appears to be because the model grid and algorithm have the same symmetries as the initial

Rossby–Haurwitz wave, so that neither truncation nor roundoff errors project onto the unstable mode; however, the stronger numerical damping in the UV semi-Lagrangian model compared to the other models may also help suppress the instability.

6. Acknowledgements

YL was supported by NASA grant 578-41-16-20.

REFERENCES

Baines, P. G. 1976. The stability of planetary waves on a sphere. *J. Fluid Mech.* **73**, 193–213.

Bates, J. R., Moorthi, S. and Higgins, R. W. 1993. A global multilevel atmospheric model using a vector semi-Lagrangian finite-difference scheme. Part 1: Adiabatic formulation. *Mon. Wea. Rev.* **121**, 244–263.

Bates, J. R., Li, Y., Brandt, A., McCormick, S. F. and Ruge, J. 1995. A global shallow-water numerical model based on the semi-Lagrangian advection of potential vorticity. *Quart. J. Roy. Meteorol. Soc.* **121**, 1981–2005.

Bates, J. R. and Li, Y., 1997. Simulation of stratospheric vortex erosion using three different global shallow water numerical models. *Atmos.-Ocean* **35**, 55–74.

Drazin, P. G. and Reid, W. H. 1981. *Hydrodynamic stability*. Cambridge University Press, Cambridge, London, New York, New Rochelle, Melbourne, Sydney, 527 pp.

Haurwitz, B. 1940. The motion of atmospheric disturbances on a spherical earth. *J. Marine Res.* **3**, 254–267.

Hoskins, B. J. 1973. Stability of the Rossby–Haurwitz wave. *Quart. J. Roy. Meteorol. Soc.* **99**, 723–745.

Jakob, R., Hack, J. J. and Williamson, D. L. 1993. *Solutions to the shallow water test set using the spectral transform method.* NCAR Technical Note TN-388+STR, National Center for Atmospheric Research, Boulder, Colorado, USA, 82 pp.

Li, Y. and Bates, J. R. 1996. A study of the behaviour of semi-Lagrangian models in the presence of orography. *Quart. J. Roy. Meteorol. Soc.* **122**, 1675–1700.

McCalpin, J. D. 1988. A quantitative analysis of the dissipation inherent in semi-Lagrangian advection. *Mon. Wea. Rev.* **116**, 2330–2336.

Phillips, N. A. 1959. Numerical integration of the primitive equations on the hemisphere. *Mon. Wea. Rev.* **87**, 333–345.

Semazzi, F. H. M. and Dekker, P. 1994. Optimal accuracy in semi-Lagrangian models. Part 1: Linear formulation. *Mon. Wea. Rev.* **122**, 2139–2159.

Thuburn, J. 1995. Dissipation and cascades to small scales in numerical models using a shape-preserving advection scheme. *Mon. Wea. Rev.* **123**, 1888–1903.

Thuburn, J. 1997. A PV-based shallow water model on a hexagonal–icosahedral grid. *Mon. Wea. Rev.* **125**, 2328–2347.

Williamson, D. L., Drake, J. B., Hack, J. J., Jakob, R. and Swarztrauber, P. N. 1992. A standard test set for numerical approximations to the shallow water equations in spherical geometry. *J. Comput. Phys.* **102**, 211–224.